Effects of environment on flavin reactivity in morphinone reductase: analysis of enzymes displaying differential charge near the N-1 atom and C-2 carbonyl region of the active-site flavin

Daniel H. CRAIG*[1], Terez BARNA*, Peter C. E. MOODY*, Neil C. BRUCE†, Stephen K. CHAPMAN‡, Andrew W. MUNRO* and Nigel S. SCRUTTON*[2]

*Department of Biochemistry and Centre for Chemical Biology, University of Leicester, University Road, Leicester LE1 7RH, U.K., †Institute of Biotechnology, University of Cambridge, Tennis Court Road, Cambridge CB2 1QT, U.K., and ‡Department of Chemistry, University of Edinburgh, The King's Buildings, West Mains Road, Edinburgh EH9 3JJ, U.K.

The side chain of residue Arg^{238} in morphinone reductase (MR) is located close to the N-1/C-2 carbonyl region of the flavin isoalloxazine ring. During enzyme reduction negative charge develops in this region of the flavin. The positioning of a positively charged side chain in the N-1/C-2 carbonyl region of protein-bound flavin is common to many flavoprotein enzymes. To assess the contribution made by Arg^{238} in stabilizing the reduced flavin in MR we isolated three mutant forms of the enzyme in which the position of the positively charged side chain was retracted from the N-1/C-2 carbonyl region ($Arg^{238} \rightarrow Lys$), the positive charge was removed ($Arg^{238} \rightarrow Met$) or the charge was reversed ($Arg^{238} \rightarrow Glu$). Each mutant enzyme retains flavin in its active site. Potentiometric studies of the flavin in the wild-type and mutant forms of MR indicate that the flavin semiquinone is not populated to any appreciable extent. Reduction of the flavin in each enzyme is best described by a single Nernst function, and the values of the midpoint reduction potentials (E_{12}) for each enzyme fall within the region of -247 ± 10 mV. Stopped-flow studies of NADH binding to wild-type and mutant MR enzymes reveal differences in the kinetics of formation and decay of an enzyme–NADH charge-transfer complex, reflecting small perturbations in active-site geometry. Reduced rates of hydride transfer in the mutant enzymes are attributed to altered geometrical alignment of the nicotinamide coenzyme with FMN rather than major perturbations in reduction potential, and this is supported by an observed entropy–enthalpy compensation effect on the hydride transfer reaction throughout the series of enzymes. The data indicate, in contrast with dogma, that the presence of a positively charged side chain close to the N-1/C-2 carbonyl region of the flavin in MR is not required to stabilize the reduced flavin. This finding may have general implications for flavoenzyme catalysis, since it has generally been assumed that positive charge in this region has a stabilizing effect on the reduced form of flavin.

Key words: flavin redox chemistry, flavoprotein, Old Yellow Enzyme family, potentiometry.

INTRODUCTION

Bacterial morphinone reductase (MR) from *Pseudomonas putida* is a member of the Old Yellow Enzyme (OYE) family of proteins [1,2]. MR catalyses the NADH-dependent saturation of the C=C double bond of both morphinone and codeinone. The enzyme is a dimer with a molecular mass of 82200 Da [1], and the structure of the enzyme has been solved by X-ray crystallography (T. Barna, C. Petroza, D. H. Craig, N. C. Bruce, N. S. Scrutton and P. C. E. Moody, unpublished work). Many aspects of the active-site structure of MR resemble those of OYE [3] and pentaerythritol tetranitrate (PETN) reductase [4]; the flavin contact residues are conserved among the three enzymes (Figure 1). A number of targeted mutations have been made in OYE around the FMN centre. Mutagenesis studies involving residues His^{191} and Asn^{194} have revealed their role in binding phenolic ligands and enzyme reduction by nicotinamide coenzymes [5]. The exchange of Tyr^{196} in OYE (which is conserved in PETN reductase, but not in MR) for Phe^{196} substantially impairs the oxidative half-reaction. This has led to the proposal that Tyr^{196} serves as a proton donor in OYE [6]. Residues that contact the FMN isoalloxazine ring probably play a major role in setting the redox potential of the flavin. Thr^{37} in OYE [conserved in MR (Thr^{32}) and PETN reductase (Thr^{26})] forms a hydrogen bond to the C-4 carbonyl of the flavin isoalloxazine. Its exchange for alanine in OYE results in a destabilization of the reduced flavin by 33 mV, and, in contrast with wild-type enzyme, the flavin semiquinone is not populated during reductive titration [7]. Consistent with this change in flavin reduction potential, the reductive half-reaction is slowed by approx. 10-fold, whereas the oxidative half-reaction is accelerated 26-fold compared with wild-type OYE. Similarly, in glycolate oxidase, mutation of Tyr^{129} to phenylalanine also perturbs the potential of the flavin, due to the removal of a hydrogen bond between the phenolic hydroxy group of Tyr^{129} and the C-4 carbonyl of the isoalloxazine ring [8].

The environment of the flavin is predicted to have a role in stabilizing the reduced forms of flavin. Reduction increases the electron density in the region of the 'enediamine' subfunction (i.e. positions N-1, C-4a and N-5) of the isoalloxazine ring, and thus the nature of the protein environment is key to modulating the reduction potential. The studies with OYE and glycolate oxidase described above have demonstrated the importance of key interactions in the C-4 carbonyl region. Extensive studies

Abbreviations used: MR, morphinone reductase; OYE, Old Yellow Enzyme; PETN, pentaerythritol tetranitrate; Q104E, R238K, R238M and R238E, $Gln^{104} \rightarrow Glu$, $Arg^{238} \rightarrow Lys$, $Arg^{238} \rightarrow Met$ and $Arg^{238} \rightarrow Glu$ respectively.

[1] Present address: Department of Chemistry, University of Edinburgh, The King's Buildings, West Mains Road, Edinburgh EH9 3JJ, U.K.

[2] To whom correspondence should be addressed (e-mail nss4@le.ac.uk).

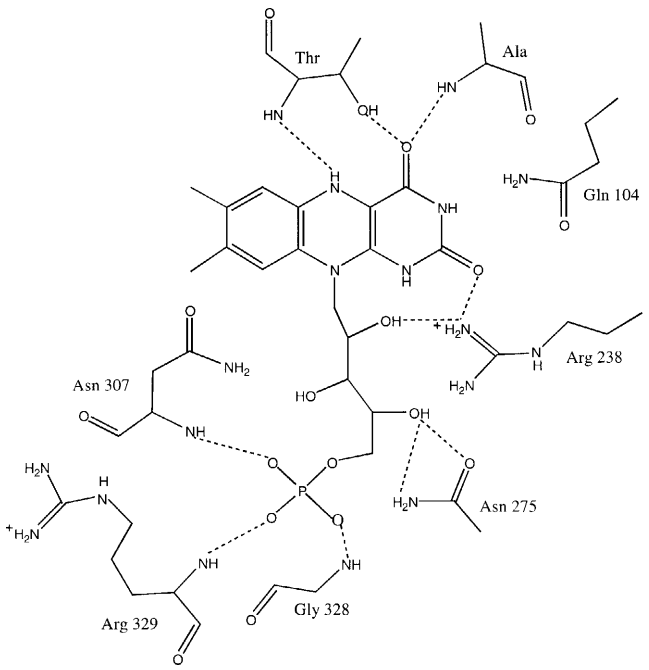

Figure 1 Molecular-graphic representation illustrating the location of residues Arg^{238} and Gln^{108} in wild-type MR in relation to the flavin isoalloxazine ring

with flavodoxins have also highlighted the importance of a hydrogen bond from a backbone carbonyl group to the flavin N-5 in stabilizing the blue (neutral) flavin semiquinone [9–12]. Hydrogen bond interactions with the N-3H of the isoalloxazine ring are also known to stabilize the semiquinone state of flavodoxins [13]. Other studies have probed the role of aromatic residues that stack on either side of the flavin in flavodoxins [14,15], and in one study, with *Methylophilus methylotrophus* electron-transferring flavoprotein, a single replacement of an arginine residue located over the face of the isoalloxazine ring resulted in an exceptional ~ 200 mV destabilization of the semiquinone form [16].

No detailed mutagenesis study has been made of the flavin environment around the N-1/C-2 carbonyl region in flavoproteins. Inspection of many flavoprotein structures reveals that a positively charged side chain is often positioned close to this region, where it is conjectured to stabilize the reduced form of the flavin. Without exception, this is the case in the FMN-binding eight-fold β/α barrel family of flavoproteins; the Class I subfamily (see [2] for definitions of subfamilies), which includes OYE, MR and PETN reductase have arginine at this position, whereas the Class II subfamily have lysine. Exchange of the arginine residue by mutagenesis in a Class I subfamily member, trimethylamine dehydrogenase, results in poor flavin binding, and this has prevented detailed potentiometric analysis [17]. Lys^{349} in the Class II subfamily member, flavocytochrome b_2, has been mutated to arginine, but no potentiometric studies have been reported [18]. The development of negative charge at the flavin N-1/C-2 carbonyl region during enzyme reduction by substrate has led to the general proposal that the positioning of a positively charged side chain close to this region of the flavin will stabilize the reduced form of the flavin isoalloxazine ring. The positioning of a positively charged residue in this region of many flavoprotein enzymes is consistent with it acting to stabilize charge development in the N-1/C-2 carbonyl region. Although this hypothesis is attractive, it has not been tested formally by the isolation and detailed characterization of appropriate site-directed mutants of flavoproteins bearing a positively charged residue in the vicinity of the flavin N-1/C-2 carbonyl region.

In the present paper we have targeted Arg^{238} in MR to probe the effect of removing a positively charged side chain from the N-1/C-2 carbonyl region of the flavin isoalloxazine ring. We have isolated three mutant forms of MR [Arg^{238} → Lys (R238K), Arg^{238} → Met (R238M) and Arg^{238} → Glu (R238E)], which were designed to displace, remove and reverse the charge respectively. We also isolated a Gln^{104} → Glu (Q104E) mutant MR to probe the environment around the N-3H position of the flavin. By potentiometry we show, in contrast with dogma, that the presence of a positively charged side chain near the N-1/C-2 carbonyl is not a requirement for stabilization of reduced flavin. Stopped-flow kinetic studies of the mutant enzymes reveal subtle changes in the reductive half-reaction that result from an altered geometry of binding of the nicotinamide coenzyme rather than perturbation of the redox potential of the flavin. Our results may have general implications for our understanding of the control of redox potential in flavoproteins.

EXPERIMENTAL

Chemicals and enzymes

Complex bacteriological media were obtained from Oxoid (Basingstoke, Hants, U.K.), and all media were prepared as described by Sambrook et al. [19]. β-NADH, 2-hydroxy-1,4-naphthoquinone, methyl viologen and benzyl viologen were purchased from Sigma.

Recombinant DNA methods and enzyme purification

Mutagenesis of the expression plasmid pMORB3 [1] encoding MR was conducted using the QuikChange site-directed mutgenesis kit from Stratagene. The following oligonucleotides (and oligonucleotides with the complementary sequences) were utilized in the mutagenesis procedure: Q104E, 5′-GGG CGC ATC GCC CTG GAG CTG TGG CAC GTC GG-3′; R238K, 5′-CCG AGC GCG TCG GCA TCA AGC TGA CCC CCT TCC TC-3′; R238M, 5′-CCG AGC GCG TCG GCA TCA TGC TGA CCC CCT TCC TC-3′; and R288E, 5′-CCG AGC GCG TCG GCA TCG AGC TGA CCC CCT TCC TC-3′. Following mutagenesis, the entire *morB* gene was re-sequenced (PerkinElmer Biosystems 377 ABI automated sequencer using BigDye terminators) to ensure spurious changes had not arisen during the mutagenesis procedure. Purification of MR mutant enzymes R238K, R238M and R238E from *Escherichia coli* strain JM109 was performed using the method previously described for the wild-type enzyme [20]. MR mutant Q104E was purified similarly, except that the Mimetic Yellow 2 affinity resin was exchanged for an ion-exchange step using DEAE (DE-52) chromatographic medium. Enzyme in buffer A [50 mM potassium phosphate (pH 7.0)/2 mM 2-mercaptoethanol] was applied on to a column of DE52 resin equilibrated in buffer A, washed (with 1 litre of buffer A) and eluted using a gradient (200 ml of buffer A containing 0–2 M KCl). Ammonium sulphate (20 %) was added to MR-containing fractions, and the enzyme was applied on to a phenyl-Sepharose column equilibrated with buffer A containing 20 % ammonium sulphate, and washed with a further 1 litre of the same buffer. Q104E MR was eluted under these conditions and judged to be pure by SDS/PAGE performed following exhaustive dialysis against buffer A.

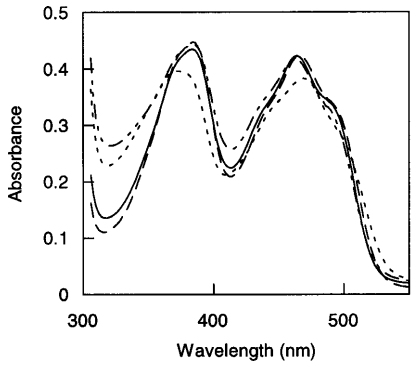

Figure 2 UV-visible absorption spectra for the purified wild-type and mutant MR enzymes

The enzymes were purified as described in the Experimental section. Conditions: 50 mM potassium phosphate buffer (pH 7.0). Continuous line, wild-type MR; large dashed lines, R238K MR; small dashed lines, R238M MR; large and small dashed lines, R238E MR.

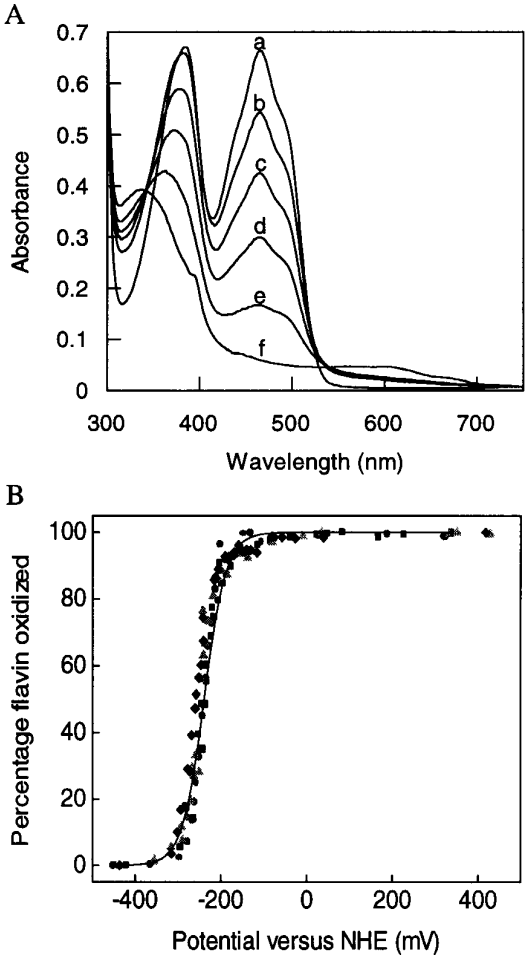

Figure 3 Potentiometric analysis of wild-type and mutant MR enzymes

(**A**) Spectral changes accompanying reductive titration of wild-type MR. Spectrum a, +339 mV; spectrum b, −207 mV; spectrum c, −233 mV; spectrum d, −253 mV; spectrum e, −294 mV; and spectrum f, −421 mV. All values are relative to the standard hydrogen electrode. (**B**) Absorbance at 465 nm versus potential, and the fit to a single Nernst function for each of the enzymes. Squares, wild-type MR; diamonds, R238K MR; triangles, R238M; circles, R238E. Values for E_{12} are given in Table 1. NHE, normal hydrogen electrode.

Redox potentiometry

Redox titrations were performed anaerobically at 25 °C inside a Belle Technology glove box as described previously [21]. Enzyme solutions were exchanged into anaerobic buffer [100 mM potassium phosphate (pH 7.0)] using a 20 cm × 1 cm Sephadex column pre-equilibrated with the same buffer. Solutions of 50–70 μM enzyme were electrochemically titrated according to the method of Dutton [22], using 5 μM 2-hydroxy-1,4-naphthoquinone, 1 μM methyl viologen and 1 μM benzyl viologen as redox mediators. The electrochemical potential of the enzyme solutions was measured at 25 ± 2 °C using a CD740 meter coupled to a Pt/calomel electrode (Russell pH Ltd, Auchtermuchty, Fife, Scotland, U.K.) that had previously been calibrated using the Fe(III)/Fe(II) couple as a standard (+108 mV); the calomel electrode was corrected by +244 ± 2 mV, relative to the normal hydrogen electrode. The absorbance of enzyme solutions throughout the redox titrations was measured using a Shimadzu 1201 UV-visible spectrophotometer and a 1 cm path-length quartz cuvette. Enzyme was titrated with dithionite solution (50 mM) until the flavin was reduced fully, and then re-oxidized by titrating with potassium ferricyanide (10 mM). Titrations were performed over a 5–8 h period; equilibration was achieved throughout the titrations and no hysteretic behaviour was observed. Corrections were made for small amounts of protein precipitation and evaporation during titrations. Corrections for precipitation were made by transforming each spectrum by a $1/\lambda$ subtraction according to eqn (1):

$$a_1 = (1-1/\lambda)[a_o-(A_{750\mathrm{n}}-A_{750\mathrm{start}})] \quad (1)$$

where a_0 and a_1 are the original and modified absorbance values at a given wavelength respectively, $A_{750\mathrm{n}}$ is the absorbance at 750 nm in the spectrum from which a_o is determined, $A_{750\mathrm{start}}$ is the absorbance value at 750 nm of the first spectrum taken before addition of dithionite, and λ is the wavelength at which a_0 is determined. Corrections for evaporation in all spectra following the oxidized spectra initially recorded were made using eqn (2):

$$a_2 = a_1\left(\frac{n_x-1}{n_{\mathrm{total}}-1}\cdot\frac{A_{\mathrm{FlavinStart}}}{A_{\mathrm{FlavinEnd}}}\right) \quad (2)$$

where a_1 and a_2 are the absorbance values modified for precipitation and then evaporation at a given wavelength, n_x is the number of the spectrum recorded in sequential order (e.g. $n_x = 2$ for the second spectrum etc.), n_{total} is the total number of spectra recorded over the entire titration, and $A_{\mathrm{FlavinStart}}$ and $A_{\mathrm{FlavinEnd}}$ are the absorbance values of the second flavin peak (at 465 nm) for the first and final oxidized spectra recorded. Data were fitted to eqn (3), which represents a concerted two-electron redox process derived by extension of the Nernst equation and the Beer–Lambert Law, as described previously [22]:

$$A_{465} = \frac{(a+b10^{(E_{12}-E)/29.5})}{1+10^{(E_{12}-E)/29.5}} \quad (3)$$

where A_{465} is the absorbance value at 465 nm at the electrode potential E, and a and b are the absorbance values of the fully oxidized and reduced enzyme at 465 nm respectively. E_{12} is the midpoint potential. Data were also fitted to eqn (4), which represents the sequential transfer of two electrons:

$$A_{465} = \frac{a10^{(E-E_1)/59}+b+c10^{(E_2-E)/59}}{1+10^{(E-E_1)/59}+10^{(E_2-E)/59}} \quad (4)$$

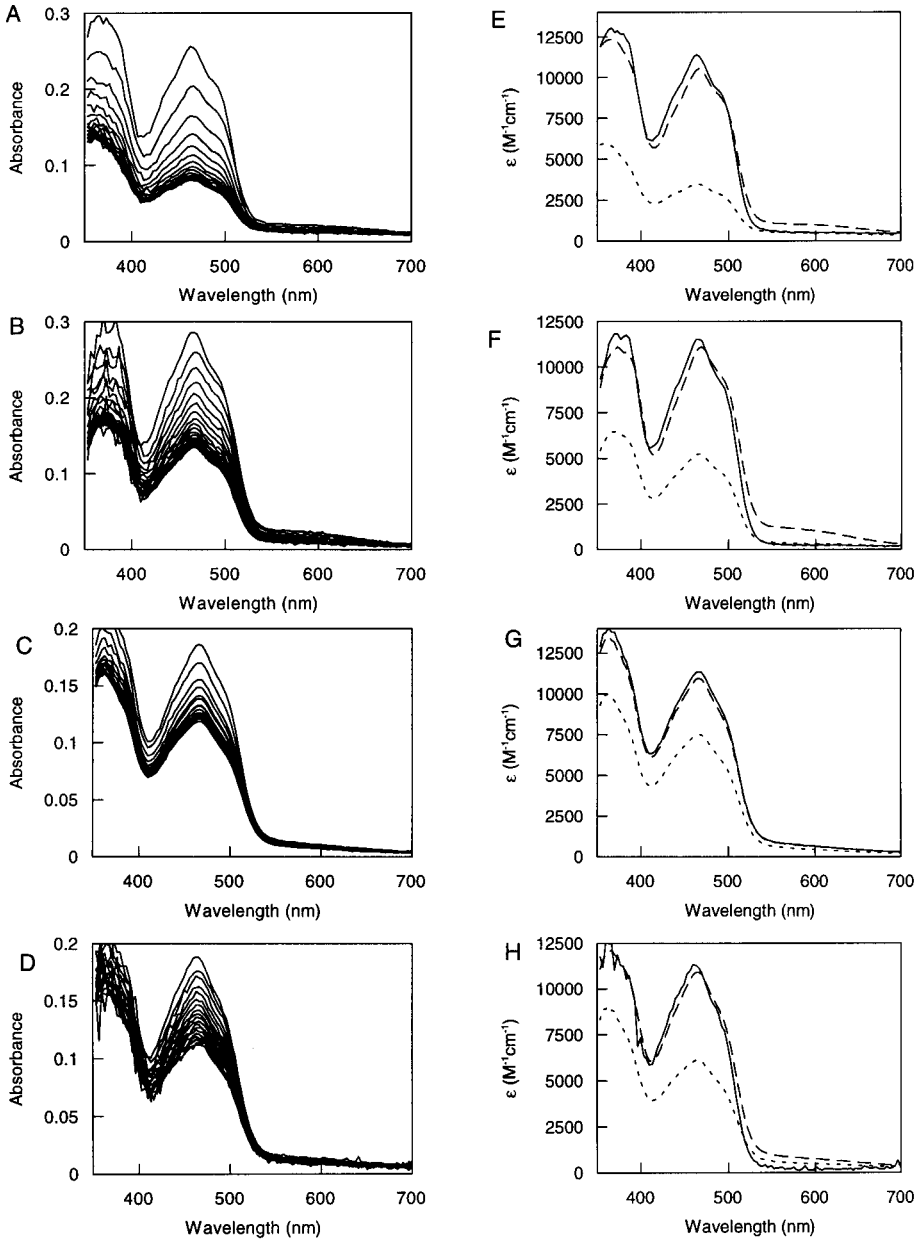

Figure 4 Multiple-wavelength photodiode array analysis of the reductive half-reactions of wild-type and mutant MR enzymes

Conditions: MR (20 μM for wild-type, 25 μM for R238K, 17 μM for R238M and 17 μM for R238E) and NADH (20 μM) were mixed at 5 °C in 50 mM potassium phosphate buffer (pH 7.0). Data acquisition was over 1 s. (**A**–**D**) Time-dependent spectral changes for wild-type (**A**), R238K (**B**), R238M (**C**) and R238E (**D**) enzymes. For clarity, not all spectra are shown. The different lines correspond to spectra of the reaction mixture at different times of the reaction. Absorption at 460 nm decreases with time. (**E**–**H**) Deconvoluted spectra obtained by fitting the data to appropriate kinetic models using PROKIN software for wild-type (**E**), R238K (**F**), R238M (**G**) and R238E (**H**). Data were fitted to an ABC model, where A is oxidized enzyme (continuous lines), B is an MR–NADH charge-transfer intermediate (dashed lines) and C is reduced enzyme (dotted lines). Strictly, spectrum C is a mixture of oxidized and reduced MR (see the text for details).

where a, b and c are absorbance coefficients for oxidized, semiquinone and reduced flavin at 465 nm respectively, E is the measured electrode potential, and E_1 and E_2 are the midpoint potentials for the oxidized/semiquinone couple and the semiquinone/reduced couple respectively. Data manipulation and analysis were performed using Origin software (Microcal). All redox potentials are given relative to the standard hydrogen electrode.

Kinetic measurements

Single turnover stopped-flow experiments were performed using an Applied Photophysics SX.18MV instrument. Time-dependent reductions of MR with NADH were performed by multiple-wavelength stopped-flow spectroscopy using a photodiode array detector and X-SCAN software (Applied Photophysics Ltd). Analysis of multiple-wavelength data using global analysis and

numerical integration methods was performed using PROKIN software (Applied Photophysics Ltd).

Analysis of stopped-flow data for wild-type MR has been presented previously [23], and the methods have been generally adopted for studies of mutant MR enzymes described in the present manuscript. Observed rate constants for flavin reduction at 462 nm following mixing with NADH were obtained by fitting kinetic transients to eqn (5):

$$A_{462} = Ce^{-k_{obs}t} + b \quad (5)$$

where C is a constant related to the initial absorbance and b is an offset value to account for a non-zero baseline. Kinetic transients at 552 nm were fitted to eqn (6):

$$A_{552} = \frac{k_{obs1}}{k_{obs2} - k_{obs1}} C(e^{-k_{obs1}t} - e^{-k_{obs2}t}) + b \quad (6)$$

where k_{obs1} and k_{obs2} are observed rates for the formation and decay of an E–NADH charge-transfer complex. Again, C is an amplitude term, t is time and b is an offset value.

RESULTS AND DISCUSSION

General properties of the mutant enzymes

Each of the mutant enzymes was purified to homogeneity as described. The absorption peak of the flavin in the R238K and R238M mutant enzymes is very slightly blue-shifted (to 464 and 466 nm respectively) compared with the wild-type enzyme and R238E mutant enzyme (462 nm) (Figure 2). The Q104E mutant enzyme was purified in the deflavo form, indicating that FMN binding in this form of MR is impaired. This mutant was isolated to probe the effect of introducing negative charge in the N-3H region of the flavin. All Class I subfamily members have glutamine in this position except for di- and tri-methylamine dehydrogenases, which have glutamate [24,25]. Based on the work of Bradley and Swenson [13], who showed that the exchange in flavodoxin of Glu[59] (which hydrogen bonds with the flavin N-3H) for glutamine resulted in a 86 mV increase in reduction potential of the semiquinone/hydroquinone couple (possibly as a result of indirect effects on the flavin N-5), the expectation was that the Q104E mutation might lead to a perturbation in reduction potential in MR. Attempts to reconstitute the Q104E MR with FMN using the acid-precipitation method described for wild-type MR [20] were unsuccessful. Far-UV CD studies revealed that the deflavo Q104E mutant retained secondary structure, indicating that the mutation did not lead to adverse effects on the structure of the enzyme (results not shown). Our data reveal, therefore, that the placement of negative charge (in the form of a glutamate residue) is incompatible with flavin binding in MR.

The ratio of absorption at 280 nm and 462–466 nm (depending on the enzyme species) for each of the R238 mutant enzymes is higher (8.7, 19 and 17 for R238K, R238M and R238E respectively) than the corresponding value (6.6) for wild-type MR, suggesting incomplete occupancy of the FMN binding site in the mutant enzymes. Full reconstitution was possible for these mutants using the acid-precipitation method described for wild-type MR [20]. Again, far-UV studies indicated that each mutant retained the dichroic signatures expected for fully folded MR.

Potentiometry

In all cases, titrations were initiated from fully oxidized wild-type and mutant MR enzymes, and proceeded gradually to the end-

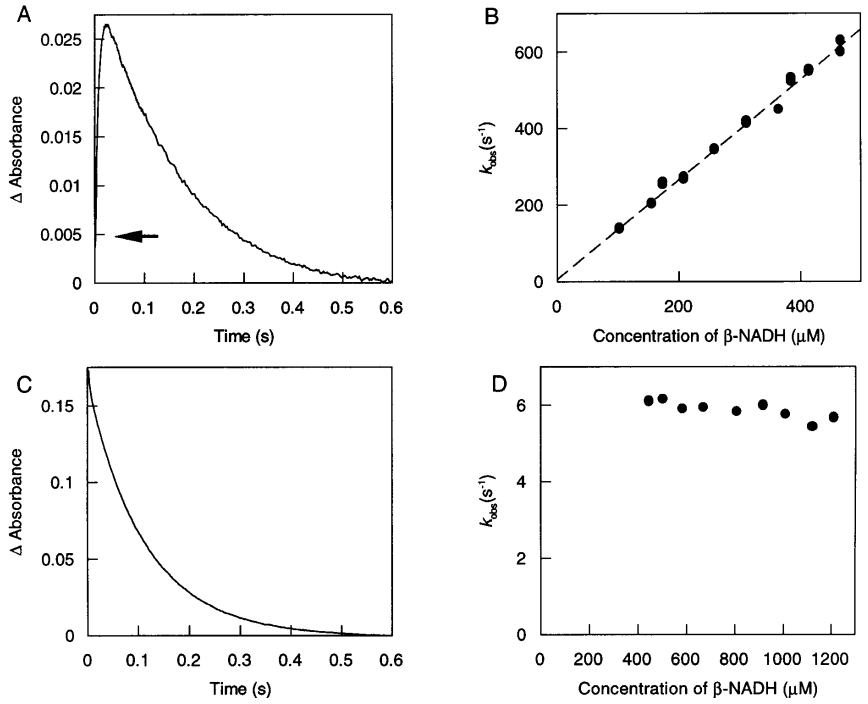

Figure 5 Transients observed for the reaction of R238K MR with NADH

(**A**) Transient observed at 552 nm. The arrow signifies the start of the transient immediately after mixing in the stopped-flow instrument. (**B**) NADH concentration-dependence of the rate of formation of the MR–NADH charge-transfer complex. (**C**) Transient observed at 462 nm. (**D**) NADH concentration-dependence of the rate of flavin reduction. Conditions: 20 μM MR, 100 μM NADH, 5 °C and 50 mM potassium phosphate buffer (pH 7.0).

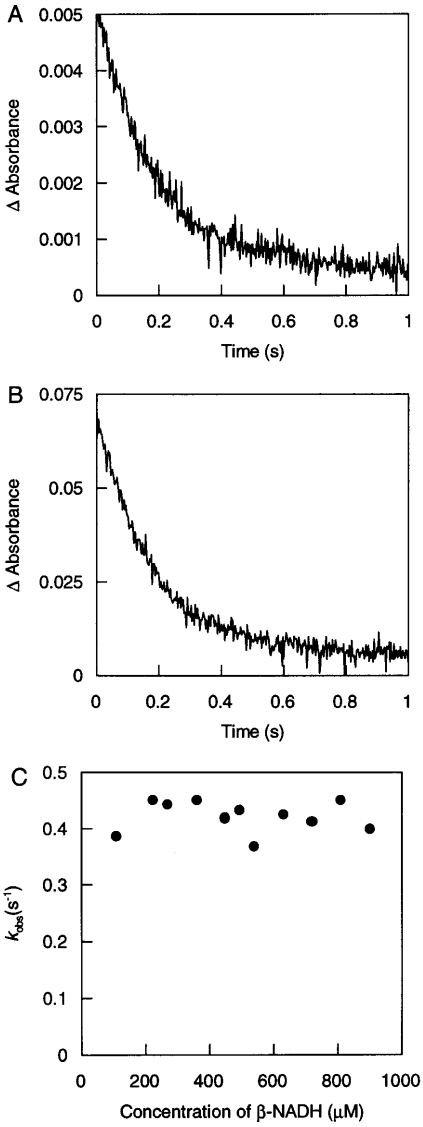

Figure 6 Transients observed for the reaction of R238M MR with NADH

(**A**) Transient observed at 552 nm. (**B**) Transient observed at 462 nm. (**C**) NADH concentration-dependence of the rate of flavin reduction. Conditions as in Figure 5.

point of the titration by the addition of small aliquots of sodium dithionite (from 50 mM stock solution), and then back again to oxidized electron-transferring protein by addition of aliquots of potassium ferricyanide (10 mM stock solution). The protein samples remained almost completely soluble and stable throughout the course of the titration, enabling collection of good quality sets of spectra. No hysteretic effects were observed in any of the redox titrations. Spectra recorded at similar potentials during oxidative and reductive titrations were essentially identical. Representative spectra for the reductive titrations of wild-type MR are shown in Figure 3(A), and plots of the percentage of flavin oxidized versus potential are shown in Figure 3(B) for wild-type MR along with the corresponding plots of the percentage of flavin oxidized versus potential for each of the mutant enzymes (Figure 3B).

Evidence for the population of a semiquinone species during reductive and oxidative titrations was not obtained, and a good fit of the data was obtained to eqn (3), which describes a concerted two-electron reduction of the enzyme. The midpoint reduction potentials for the wild-type and mutant MR enzymes are presented in Table 1. Good fits of the data were also obtained for a double Nernst function (i.e. sequential two-electron transfer). However, although the double Nernst function accurately calculates coefficients for the fully oxidized and fully reduced forms of the enzymes, the coefficient for the flavin semiquinone is not estimated reproducibly for the different enzymes. The double Nernst function gives estimates of E_1 (oxidized/semiquinone couple) and E_2 (semiquinone/hydroquinone couple) that are very close. The errors in the potentials determined by this method mean that, in most cases, the E_1 and E_2 values are close to overlapping, indicating that the two-electron function cannot distinguish accurately between the E_1 and E_2 values. However, the most notable exception is the R238E enzyme, where the double Nernst function resolves the two redox couples satisfactorily ($E_1 = -264 \pm 6$ and $E_2 = -222 \pm 7$ mV). The more positive potential of the semiquinone/dihydroquinone couple is as expected for a situation where insignificant visible semiquinone is formed during the redox titration. However, the E_{12} value (-247 ± 10 mV for all enzymes investigated; see Table 1 for individual enzyme values) is determined accurately from a single Nernst function. The data indicate that, at best, only very small quantities of semiquinone accumulate in any of the titrations. The signals for any small quantities of red anionic semiquinone will be buried under the remaining oxidized flavin absorbance. The potentiometry data clearly indicate that relocation of the positive charge (R238K), removal of the positive charge (R238M) and reversal of charge (R238E) have surprisingly little effect on the stability of the reduced flavin in MR. One possible explanation is that protonation of the flavin N-1 ($pK_a = 6.7$ for free flavin) may neutralize the charge developed on the flavin N-1 in the mutant enzymes when stabilization from the side chain of residue 238 is not possible. This possibility will be explored in future work by NMR methods employing wild-type and mutant MR enzymes in which FMN is replaced with ^{15}N-enriched FMN.

Table 1 Midpoint reduction potentials (E_{12}) determined for wild-type and mutant MR enzymes by fitting to single Nernst functions

Enzyme	E_{12} (mV)
Wild-type	-237 ± 6
R238K	-257 ± 6
R238M	-249 ± 6
R238E	-240 ± 4

Multiple-wavelength kinetic analyses of flavin reduction by NADH

To gain further insight into the effects of the mutations introduced at position 238 on the properties of MR, we conducted stopped-flow analysis of FMN reduction by NADH. The analyses are an extension of the kinetic and thermodynamic studies we performed previously on wild-type MR, and detailed kinetic modelling of the reaction catalysed by MR can be found in a previous publication [23]. All reactions were performed under anaerobic conditions to prevent enzyme re-oxidation by molecular oxygen. Multiple-wavelength analysis of stoichiometric reactions of MR with NADH is displayed in Figure 4. Reaction conditions were chosen to slow the formation of charge-transfer species between MR and NADH. Under pseudo first-order conditions the rate of formation of the MR–NADH charge-transfer species is too fast

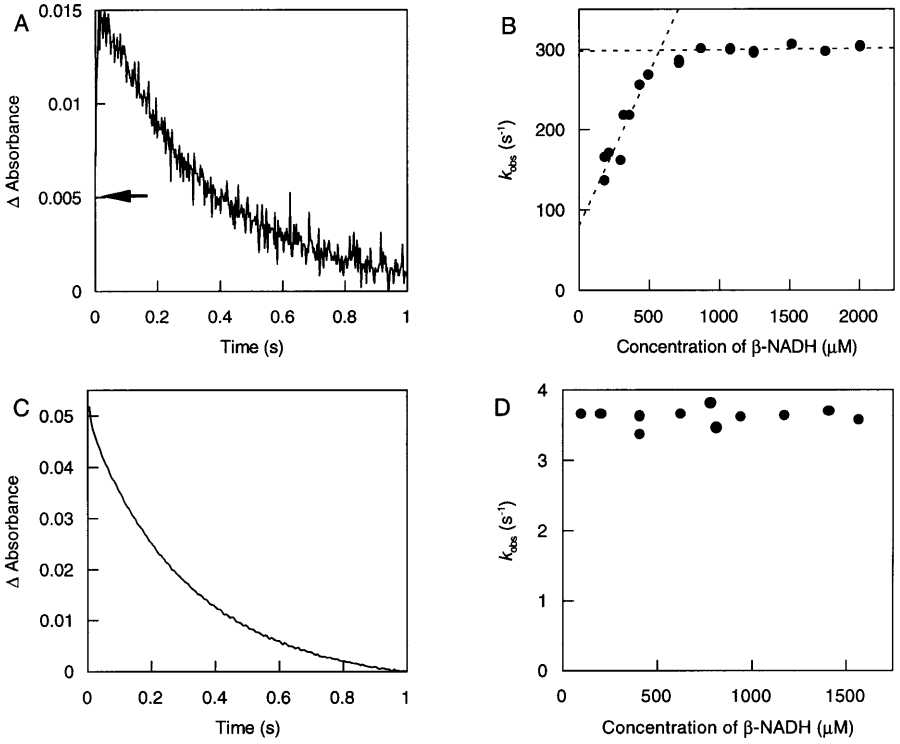

Figure 7 Transients observed for the reaction of R238E MR with NADH

(**A**) Transient observed at 552 nm. (**B**) NADH concentration-dependence of the rate of formation of the MR–NADH charge-transfer complex. (**C**) Transient observed at 462 nm. (**D**) NADH concentration-dependence of the rate of flavin reduction. Conditions as in Figure 5.

to enable capture of the rapid absorption changes using the photodiode array detector. As seen previously with wild-type MR [23], the development of an MR–NADH charge-transfer species is seen at long wavelengths prior to flavin reduction in both the R238K and R238E mutant enzymes; the long-wavelength absorption is most intense in the R238K enzyme. Data obtained for R238M MR suggest that the charge-transfer intermediates form in the dead time of the stopped-flow instrument; during data acquisition a small decrease in absorption is seen at approx. 550–600 nm, consistent with the decay of a charge-transfer intermediate concomitant with flavin reduction. The different final reduction levels of the flavin for each of the enzymes at the end of data acquisition are not due to perturbation of redox potential. Data acquisition using our photodiode array detector does not allow spectral acquisition in 'split' or 'log' time-base mode. Consequently, to enable capture of the fast absorption changes associated with formation of the charge-transfer complex, data acquisition was restricted to 1 s. In this time period, reduction of the flavin in the mutant enzymes (particularly R238M and R238E) is less complete than in the wild-type enzyme, owing to the slower rates of hydride transfer in these enzymes (see below).

Single-wavelength kinetic studies

Single-wavelength stopped-flow studies were conducted to investigate the dependence of the rate of flavin reduction and the rate of formation of the MR–NADH charge-transfer complex on NADH concentration. R238K MR behaves qualitatively the same as the wild-type enzyme: reaction transients at 552 nm are biphasic, reporting on formation and then decay of the MR–NADH charge-transfer complex, and transients at 462 nm are monophasic, reporting on flavin reduction (Figure 5). From Figure 5(B), the second-order rate constant for formation of the charge-transfer complex is $13 \times 10^5\ M^{-1} \cdot s^{-1}$ (compared with $4.8 \times 10^5\ M^{-1} \cdot s^{-1}$ for wild-type [23]). The intercept value indicates that decay of the MR–NADH charge-transfer complex to form MR and NADH occurs at a rate of 5.6 s^{-1} (80 s^{-1} for wild-type) and the K_d for the MR–NADH complex is 4.3 μM (166 μM for wild-type). The rate of flavin reduction in R238K MR (6 s^{-1}) is independent of NADH concentration (Figure 5D) and compares with a value of 18 s^{-1} for wild-type enzyme [23].

$$EFl_{ox} + NADH \underset{k_{-1}}{\overset{k_1}{\rightleftharpoons}} EFl_{ox}\text{-}NADH \underset{k_{-2}}{\overset{k_2}{\rightleftharpoons}} EFl_{ox}\text{-}NADH^{CT} \underset{k_{-3}}{\overset{k_3}{\rightleftharpoons}} EFl_{red} + NAD^+$$

Scheme 1 Kinetic scheme for the reductive half-reaction of MR

EFl, enzyme–flavin complex; CT, charge-transfer complex.

Single-wavelength transients for R238M MR are illustrated in Figure 6. At 552 nm a monophasic absorption decrease is seen with the same kinetics as the absorption decrease observed at 462 nm. This probably represents the decay of a MR–NADH charge-transfer complex that forms within the dead time of the stopped-flow instrument. At both wavelengths, observed rates (0.4 s^{-1}), which report on flavin reduction, were independent of NADH concentration (Figure 6C), which again lends support to the development of a discrete charge-transfer intermediate (the rate of formation of which would be dependent on NADH concentration).

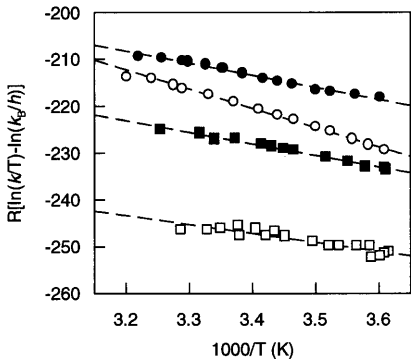

Figure 8 Thermodynamic analysis of hydride transfer in wild-type and mutant MR enzymes

Conditions: 20 μM MR, 100 μM NADH and 50 mM potassium phosphate buffer (pH 7.0). ●, Wild-type MR; ○, R238K MR; ■, R238E MR; and □, R238M MR. Thermodynamic parameters are given in Table 2.

Table 2 Thermodynamic parameters associated with the hydride transfer reaction for wild-type and mutant MR enzymes

The $\Delta G^{\ddagger}$ values were calculated at 298 K.

Enzyme	$\Delta S^{\ddagger}$ (J·mol^{-1}·K^{-1})	$\Delta H^{\ddagger}$ (kJ·mol^{-1})	$\Delta G^{\ddagger}$ (kJ·mol^{-1})
Wild-type	−125.9 ± 2.7	25.7 ± 0.8	63.2 ± 1.6
R238K	−81.1 ± 2.0	40.5 ± 0.6	65.1 ± 1.2
R238M	−182.2 ± 6.8	19.1 ± 1.9	73.2 ± 3.9
R238E	−144.0 ± 2.8	24.7 ± 0.8	67.6 ± 1.6

Mutant R238E displayed the widest divergence from the behaviour of wild-type MR. Single-wavelength transients at 552 nm and 462 nm are displayed in Figures 7(A) and 7(C) respectively. From Figure 7(A) it can be seen that formation and decay of the charge-transfer complex are captured in the stopped-flow experiment; decay of the charge-transfer species is concomitant with flavin reduction observed at 462 nm (Figure 7C). The observed rate of flavin reduction (3.6 s^{-1}) is independent of NADH concentration (Figure 7D). In contrast with wild-type MR and the R238K and R238M mutant enzymes, however, the rate of formation of the MR–NADH charge-transfer species was not linearly dependent on NADH concentration (Figure 7B) and approached a limiting value of 300 s^{-1}. The data are best described by the kinetic model shown in Scheme 1, which invokes the existence of an MR–NADH complex that then rapidly isomerizes to form the MR–NADH charge-transfer complex. A precedent for this type of mechanism is available from studies with OYE in its reaction with nicotinamide coenzymes [26]. In Scheme 1, when $k_2 > k_{-1}$ and at low NADH concentrations, formation of the charge-transfer complex is second-order. At higher NADH concentrations the dependence becomes first-order (and thus independent of NADH concentration) as k_2 becomes rate-limiting.

Thermodynamic analysis of flavin reduction

Observed rate constants for flavin reduction were measured over the temperature range 3.4–38 °C and analysed in terms of the unimolecular rate law written in the following form [eqn (7)]:

$$R\left[\ln\left(\frac{k}{T}\right)-\ln\left(\frac{k_B}{h}\right)\right]=\Delta S^{\ddagger}-\Delta H^{\ddagger}\left(\frac{1}{T}\right) \quad (7)$$

where R is the gas constant, T is absolute temperature, k is the rate constant for flavin reduction, k_B is the Boltzmann constant, h is Planck's constant, $\Delta S^{\ddagger}$ is the change in entropy and $\Delta H^{\ddagger}$ is the change in enthalpy on moving from the ground state to the transition state of the reaction (the double dagger symbol indicates the transition state of a chemical reaction).

The temperature dependence of the rate of flavin reduction is presented in Figure 8, and the thermodynamic parameters are given in Table 2. Although the free energy change for hydride transfer from the nicotinamide coenzyme to N-5 of FMN is similar for the wild-type and mutant enzymes, there is more variation in the entropic and enthalpic contributions to the reaction. Entropy–enthalpy compensation effects of this type are common and are often associated with changes in protein conformation associated with ligand binding or limited mutagenesis, and reflect the balance between disorganization within the active site and effective binding [27].

Taken together, our data indicate that Arg^{238} contributes little to the stabilization of the reduced forms of the FMN prosthetic group in MR. Mutagenesis of this residue clearly affects the kinetics of flavin reduction, but this is most likely attributed to altered geometry of binding of the nicotinamide with respect to the flavin isoalloxazine ring. Our kinetic studies with the R238E mutant MR have also identified an additional intermediate in the reductive half-reaction prior to formation of the charge-transfer complex, which mirrors similar findings in wild-type OYE. The entropy–enthalpy compensation effects observed for the hydride transfer step in the reductive half-reaction support altered geometries of binding. Our findings may have general implications for flavoenzyme catalysis, since it has been assumed that the positioning of positive charge close to the N-1/C-2 carbonyl region of a protein-bound flavin will assist in reduction by stabilizing the reduced form of the flavin. However, the general discrediting of this hypothesis must await the outcome of similar mutagenesis studies on alternative flavoenzymes. By extending these studies to other flavoenzymes, the general significance of the influence of cationic charge at the N-1/C-2 carbonyl region (and its removal), and the effects on the ionization state of the N-1 atom will become apparent. These studies will further strengthen the impact of our observations made with MR on the lack of a significant role for cationic change on flavin reactivity.

This work was funded by a grant from the Biotechnology and Biological Sciences Research Council. N.S.S. is a Lister Institute Research Professor.

REFERENCES

1 French, C. E. and Bruce, N. C. (1995) Bacterial morphinone reductase is related to Old Yellow Enzyme. Biochem. J. **312**, 671–678
2 Scrutton, N. S. (1994) Alpha/beta barrel evolution and the modular assembly of enzymes: emerging trends in the flavin oxidase/dehydrogenase family. BioEssays **16**, 115–122
3 Fox, K. M. and Karplus, P. A. (1994) Old yellow enzyme at 2 Å resolution: overall structure, ligand binding, and comparison with related flavoproteins. Structure (London) **2**, 1089–1105
4 Barna, T., Khan, H., Bruce, N. C., Scrutton, N. S. and Moody, P. C. E. (2001) Crystal structure of pentaerythritol tetranitrate reductase: 'flipped' binding geometries for steroid substrates in different redox states of the enzyme. J. Mol. Biol. **310**, 433–447
5 Brown, B. J., Deng, Z., Karplus, P. A. and Massey, V. (1998) On the active site of Old Yellow Enzyme. Role of histidine 191 and asparagine 194. J. Biol. Chem. **273**, 32753–32762

6 Kohli, R. M. and Massey, V. (1998) The oxidative half-reaction of Old Yellow Enzyme. The role of tyrosine 196. J. Biol. Chem. **273**, 32763–32770

7 Xu, D., Kohli, R. M. and Massey, V. (1999) The role of threonine 37 in flavin reactivity of the old yellow enzyme. Proc. Natl. Acad. Sci. U.S.A. **96**, 3556–3561

8 Macheroux, P., Kieweg, V., Massey, V., Soderlind, E., Stenberg, K. and Lindqvist, Y. (1993) Role of tyrosine 129 in the active site of spinach glycolate oxidase. Eur. J. Biochem. **213**, 1047–1054

9 Ludwig, M. L., Pattridge, K. A., Metzger, A. L., Dixon, M. M., Eren, M., Feng, Y. and Swenson, R. P. (1997) Control of oxidation-reduction potentials in flavodoxin from *Clostridium beijerinckii*: the role of conformation changes. Biochemistry **36**, 1259–1280

10 O'Farrell, P. A., Walsh, M. A., McCarthy, A. A., Higgins, T. M., Voordouw, G. and Mayhew, S. G. (1998) Modulation of the redox potentials of FMN in *Desulfovibrio vulgaris* flavodoxin: thermodynamic properties and crystal structures of glycine-61 mutants. Biochemistry **37**, 8405–8416

11 Chang, F. C. and Swenson, R. P. (1999) The midpoint potentials for the oxidized-semiquinone couple for Gly57 mutants of the *Clostridium beijerinckii* flavodoxin correlate with changes in the hydrogen-bonding interaction with the proton on N(5) of the reduced flavin mononucleotide cofactor as measured by NMR chemical shift temperature dependencies. Biochemistry **38**, 7168–7176

12 Kasim, M. and Swenson, R. P. (2000) Conformational energetics of a reverse turn in the *Clostridium beijerinckii* flavodoxin is directly coupled to the modulation of its oxidation-reduction potentials. Biochemistry **39**, 15322–15332

13 Bradley, L. H. and Swenson, R. P. (1999) Role of glutamate-59 hydrogen bonded to N(3)H of the flavin mononucleotide cofactor in the modulation of the redox potentials of the *Clostridium beijerinckii* flavodoxin. Glutamate-59 is not responsible for the pH dependency but contributes to the stabilization of the flavin semiquinone. Biochemistry **38**, 12377–12386

14 Lostao, A., Gomez-Moreno, C., Mayhew, S. G. and Sancho, J. (1997) Differential stabilization of the three FMN redox forms by tyrosine 94 and tryptophan 57 in flavodoxin from *Anabaena* and its influence on the redox potentials. Biochemistry **36**, 14334–14344

15 Chang, F. C. and Swenson, R. P. (1997) Regulation of oxidation-reduction potentials through redox-linked ionization in the Y98H mutant of the *Desulfovibrio vulgaris* [Hildenborough] flavodoxin: direct proton nuclear magnetic resonance spectroscopic evidence for the redox-dependent shift in the pKa of Histidine-98. Biochemistry **36**, 9013–9021

16 Talfounier, F., Munro, A. W., Basran, J., Daff, S., Sutcliffe, M. J., Chapman, S. K. and Scrutton, N. S. (2001) αArg-237 in *Methylophilus methylotrophus* (sp. W3A1) electron-transferring flavoprotein affords ~ 200 mV stabilization of the FAD anionic semiquinone and a kinetic block on full reduction to the dihydroquinone. J. Biol. Chem. **276**, 20190–20196

17 Mewies, M., Packman, L. C., Mathews, F. S. and Scrutton, N. S. (1996) Flavinylation in wild-type trimethylamine dehydrogenase and differentially charged mutant enzymes: a study of the protein environment around the N1 of the flavin isoalloxazine. Biochem. J. **317**, 267–272

18 Reid, G. A., White, S., Black, M. T., Lederer, F., Mathews, F. S. and Chapman, S. K. (1988) Probing the active site of flavocytochrome b2 by site-directed mutagenesis. Eur. J. Biochem. **178**, 329–333

19 Sambrook, J., Fritsch, E. and Maniatis, T. (1989) Molecular Cloning: A Laboratory Manual, 2nd edn, Cold Spring Harbor Laboratory Press, Cold Spring Harbor, NY

20 French, C. E. and Bruce, N. C. (1994) Purification and characterization of morphinone reductase from *Pseudomonas putida* M10. Biochem. J. **301**, 97–103

21 Daff, S. N., Chapman, S. K., Turner, K. L., Holt, R. A., Govindaraj, S., Poulos, T. L. and Munro, A. W. (1997) Redox control of the catalytic cycle of flavocytochrome P-450 BM3. Biochemistry **36**, 13816–13823

22 Dutton, P. (1978) Redox potentiometry: determination of midpoint potentials of oxidation-reduction components of biological electron-transfer systems. Methods Enzymol. **54**, 411–435

23 Craig, D. H., Moody, P. C. E., Bruce, N. C. and Scrutton, N. S. (1998) Reductive and oxidative half-reactions of morphinone reductase from *Pseudomonas putida* M10: a kinetic and thermodynamic analysis. Biochemistry **37**, 7598–7607

24 Boyd, G., Mathews, F. S., Packman, L. C. and Scrutton, N. S. (1992) Trimethylamine dehydrogenase of bacterium W3A1. Molecular cloning, sequence determination and over-expression of the gene. FEBS Lett. **308**, 271–276

25 Yang, C. C., Packman, L. C. and Scrutton, N. S. (1995) The primary structure of *Hyphomicrobium* X dimethylamine dehydrogenase. Relationship to trimethylamine dehydrogenase and implications for substrate recognition. Eur. J. Biochem. **232**, 264–271

26 Massey, V. and Schopfer, L. M. (1986) Reactivity of old yellow enzyme with alpha-NADPH and other pyridine nucleotide derivatives. J. Biol. Chem. **261**, 1215–1222

27 Qian, H. (1998) Entropy-enthalpy compensation: conformational fluctuation and induced-fit. J. Chem. Phys. **109**, 10015–10017

Received 27 April 2001/25 June 2001; accepted 2 August 2001